Published in final edited form as:
JACC Cardiovasc Imaging. 2008 September ; 1(5): 624–634. doi:10.1016/j.jcmg.2008.06.003.

Antiangiogenic Synergism of Integrin-Targeted Fumagillin Nanoparticles and Atorvastatin in Atherosclerosis

Patrick M. Winter, PhD[*], **Shelton D. Caruthers, PhD**[*,†], **Huiying Zhang**[*], **Todd A. Williams**[*], **Samuel A. Wickline, MD FACC**[*], and **Gregory M. Lanza, MD PhD FACC**[*]

[*]*Washington University, St. Louis, MO*

[†]*Philips Healthcare, Andover, MA*

Abstract

OBJECTIVE—Studies were performed to develop a prolonged antiangiogenesis therapy regimen based on theranostic $\alpha_v\beta_3$–targeted nanoparticles.

BACKGROUND—Antiangiogenesis therapy may normalize atherosclerotic plaque vasculature and promote plaque stabilization.$\alpha_v\beta_3$–targeted paramagnetic nanoparticles can quantify atherosclerotic angiogenesis and incorporate fumagillin to elicit acute antiangiogenic effects.

METHODS—In the first experiment, hyperlipidemic rabbits received $\alpha_v\beta_3$–targeted fumagillin nanoparticles (0, 30, or 90 μg/kg) with either a continued high fat diet or conversion to standard chow. The antiangiogenic response was followed for 4 weeks by MR molecular imaging with $\alpha_v\beta_3$–targeted paramagnetic nanoparticles. In a second 8-week study, atherosclerotic rabbits received atorvastatin (0 or 44 mg/kg diet) alone or with $\alpha_v\beta_3$–targeted fumagillin nanoparticles (only week 0 vs. weeks 0 and 4), and angiogenesis was monitored with MR molecular imaging. Histology was performed to determine the location of bound nanoparticles and to correlate the level of MRI enhancement with the density of angiogenic vessels.

RESULTS—$\alpha_v\beta_3$–targeted fumagillin nanoparticles reduced the neovascular signal by 50 to 75% at 1-week, and maintained this effect for 3 weeks regardless of diet and drug dose. In the second study, atherosclerotic rabbits receiving statin alone had no antineovascular benefit over 8 weeks. $\alpha_v\beta_3$–targeted fumagillin nanoparticles decreased aortic angiogenesis for 3 weeks as in study one and readministration on week 4 reproduced the 3-week antineovascular response with no carry over benefit. However, atorvastatin and two doses of $\alpha_v\beta_3$–targeted fumagillin nanoparticles (0 and 4 weeks) achieved marked and sustainable antiangiogenesis. Microscopic studies corroborated the high correlation between MR signal and neovessel counts and confirmed that the $\alpha_v\beta_3$-targeted nanoparticles were constrained to the vasculature of the aortic adventia.

CONCLUSION—MR molecular imaging with $\alpha_v\beta_3$–targeted paramagnetic nanoparticles demonstrated that the acute antiangiogenic effects of $\alpha_v\beta_3$–targeted fumagillin nanoparticles could

Correspondence: Dr. Gregory M. Lanza, MD PhD or Dr. Patrick M. Winter, PhD, Washington University School of Medicine, 4320 Forest Park Avenue, CORTEX Building, Suite 101, Campus Box 8125, St. Louis, MO 63108, Tele: 314-454-8635, Fax: 314-454-5265, Email: greg@cvu.wustl.edu or patrick@cvu.wustl.edu, Web: http://cmrl.wustl.edu.

Disclosures Dr. Winter is a consultant to Kereos Inc. (St. Louis, MO). Dr. Caruthers is an employee of Philips Medical Systems (Andover, MA). Dr. Wickline receives equipment support from Philips Healthcare (Andover, MA). Drs. Wickline and Lanza are founders and stockholders of Kereos Inc. (St. Louis, MO).

be prolonged when combined with atorvastatin, representing a potential strategy to evaluate antiangiogenic treatment and plaque stability.

Keywords

Angiogenesis; Atherosclerosis; Molecular Imaging; Fumagillin; Nanoparticle

Atherosclerotic plaque progresses from an early atheromatous lesion to a thin-capped vulnerable plaque through aggressive inflammatory and immune responses, comprising macrophage infiltration with necrotic core enlargement, neovascular expansion of the vasa vasorum, and intraplaque hemorrhage (1-3). Increased plaque angiogenesis, driven by hypoxia (4), proangiogenic growth factors (5) and oxidative stress (6), portends unstable vascular disease (1,2). Angiogenesis is correlated with plaque rupture (1) and is associated with the morphological features of vulnerable atheromas including macrophage infiltrated fibrous caps (1), lipid-rich cores (7) and thin-cap shoulders (1). The preponderance of data from experimental models and human pathological samples indicate that plaque neovasculature could serve as a molecular imaging biomarker of atherosclerotic severity and cardiovascular disease risk.

Traditional therapies, such as HMG-CoA reductase inhibitors, have been proven to reduce cardiovascular risk (8), but their benefits may exceed the primary lipid-lowering effects. The pleiotropic benefits of statins have been attributed to antioxidant effects (9) diminished leukocyte-endothelial cell adhesion (10), attenuated macrophage activation and cytokine release (11), increased endothelial nitric oxide activity (12) or atherosclerotic plaque stabilization (13). Pathological data from excised carotid arteries of patients treated for three months with statins have revealed a reduction in microvascular density, which was proposed as an explanation for the additional benefit of statins (14). Others have asserted that direct evidence of decreased intraplaque angiogenesis attributable to statins and clinical improvement is lacking, and a normalized vasculature achieved through neovascular pruning may be less prone to intraplaque hemorrhage and promote plaque stabilization (3,15).

Three anti-VEGF drugs have been approved for use in specific cancers, but these drugs are expensive and have significant adverse effects including proteinuria, hypertension, thrombosis and intestinal perforation (16). While this risk-benefit profile is acceptable in the context of cancer patient survival, the efficacy of these or similar drugs for the chronic treatment of patients with atherosclerosis is less clear. A potent, clinically translatable antiangiogenic strategy that provides direct monitoring and treatment is needed for the chronic management of atherosclerotic patients.

We have shown that $\alpha_v\beta_3$–targeted paramagnetic nanoparticles can be used to quantify angiogenesis in atherosclerosis (17) and with the incorporation of fumagillin, this theranostic agent can deliver an acute antiangiogenic effect (18). The overarching hypothesis of these studies was to determine whether the acute benefits of $\alpha_v\beta_3$–targeted fumagillin nanoparticles could be incorporated into a clinically translatable regimen for testing the potential benefits of long-term antiangiogenesis therapy. Accordingly, the first objective of these studies was to define the antiangiogenic pharmacodynamics of a single $\alpha_v\beta_3$–targeted fumagillin nanoparticle dosage. Then secondly, to determine if the antiangiogenic effects of $\alpha_v\beta_3$–targeted fumagillin nanoparticles used acutely could be sustained with oral atorvastatin.

METHODS

$\alpha_v\beta_3$–Targeted Nanoparticle Synthesis

$\alpha_v\beta_3$–Targeted nanoparticles were prepared similar to previous reports (17-19). All nanoparticle emulsions comprised 20% (v/v) perfluorooctylbromide (Exfluor, Inc., Round Rock, TX), 1.3 to 2% (w/v) of a surfactant co-mixture, 1.7% (w/v) glycerin and water for the balance. The surfactant co-mixture for the paramagnetic nanoparticles included 69.9 mole% lecithin (Avanti Polar Lipids, Inc., Alabaster, AL), 0.1 mole% peptidomimetic $\alpha_v\beta_3$–integrin antagonist (US Patent 6,322,770) conjugated to PEG_{2000}-phosphatidylethanolamine (Avanti Polar Lipids, Inc., Alabaster, AL) and 30 mole% gadolinium diethylene-triamine-pentaacetic acid-bis-oleate (Gateway Chemical Technologies, St. Louis, MO). The fumagillin (Sigma, St. Louis, MO) was included at the proportionate expense of lecitin in the surfactant at two different levels corresponding to 30 μg or 90 μg of drug per ml of emulsion. $\alpha_v\beta_3$-Targeted rhodamine nanoparticles incorporated 0.1 mol% rhodamine phosphatidylethanolamine in the surfactant mix at the expense of lecithin for fluorescent microscopy studies.

The $\alpha_v\beta_3$–integrin antagonist used is a quinalone nonpeptide developed by Bristol-Myers Squibb Medical Imaging (US patent 6,511,648), initially reported as the ^{111}In-DOTA conjugate RP748 and cyan 5.5 homologue TA145 (20). The $\alpha_v\beta_3$–ligand has a 15-fold preference for the Mn^{2+} activated receptor (21 nmol/l) (20) and an IC_{50} for $\alpha_v\beta_5$, $\alpha_5\beta_1$, and GP IIbIIIa >10 μM (Bristol-Myers Squibb Medical Imaging, Billerica, MA, unpublished data). Nanoparticles have an IC_{50} of 50pM for the Mn^{2+} activated $\alpha_v\beta_3$–integrin (Kereos, Inc., St. Louis, MO, unpublished data).

Experimental Design

All animal care and experimental protocols were in accordance with Washington University guidelines. New Zealand White rabbits (n=37, 10-12 weeks old, Charles River Laboratories, Wilmington, MA) were fed a 0.25% cholesterol diet (Purina Mills, St. Louis, MO) for 100 days. In one study, animals either continued on the high cholesterol diet or were converted to standard chow after the targeted fumagillin treatment; however, the serum cholesterol levels remained highly elevated over the course of the study in all animals (1374 ± 67 mg/dl) independent of treatment. Therefore, in the second study, the high cholesterol diet was continued with or without atorvastatin alone or in combination with nanoparticle treatment.

STUDY ONE—The hypothesis tested in study one was whether a single pulsed dose of $\alpha_v\beta_3$–targeted fumagillin nanoparticles could persistently suppress angiogenesis in the aortic wall. Animals were randomly assigned to one of six treatment groups:

1. $\alpha_v\beta_3$–targeted, paramagnetic nanoparticles without fumagillin and 0.0% cholesterol (n=6)
2. $\alpha_v\beta_3$–targeted, paramagnetic nanoparticles without fumagillin and 0.25% cholesterol (n=8)
3. $\alpha_v\beta_3$–targeted, paramagnetic nanoparticles with fumagillin (30 μg/kg body weight) and 0.0% cholesterol (n=7)
4. $\alpha_v\beta_3$–targeted, paramagnetic nanoparticles with fumagillin (30 μg/kg body weight) and 0.25% cholesterol (n=6)
5. $\alpha_v\beta_3$–targeted, paramagnetic nanoparticles with fumagillin (90 μg/kg body weight) and 0.0% cholesterol (n=5)
6. $\alpha_v\beta_3$–targeted, paramagnetic nanoparticles with fumagillin (90 μg/kg body weight) and 0.25% cholesterol (n=5)

Therapeutic or control nanoparticles were administered IV on week 0 and MR molecular imaging of angiogenesis was repeated on weeks 1, 2, 3 and 4 using $\alpha_v\beta_3$-targeted, paramagnetic nanoparticles (no drug).

STUDY TWO—The hypothesis tested in study two was whether combinational therapy with $\alpha_v\beta_3$–targeted fumagillin nanoparticles and atorvastatin could sustain the antiangiogenic effect observed in study one. Rabbits were maintained on the 0.25% cholesterol diet throughout the study, with a portion of the animals receiving feed supplemented with atorvastatin (44 mg/kg). The following treatment combinations were studied:

1. $\alpha_v\beta_3$–targeted, paramagnetic nanoparticles without fumagillin and without atorvastatin (n=5)
2. $\alpha_v\beta_3$–targeted, paramagnetic nanoparticles without fumagillin and with atorvastatin (n=8)
3. $\alpha_v\beta_3$–targeted, paramagnetic nanoparticles with fumagillin (30 μg/kg body weight, baseline and week 4) without atorvastatin (n=5)
4. $\alpha_v\beta_3$–targeted, paramagnetic nanoparticles with fumagillin (30 μg/kg body weight, baseline) with atorvastatin (n=8)
5. $\alpha_v\beta_3$–targeted, paramagnetic nanoparticles with fumagillin (30 μg/kg body weight, baseline and week 4) with atorvastatin (n=8)

Aortic neovasculature signal was followed for 8 weeks with serial MR molecular imaging at baseline and on weeks 1, 2, 4, 6 and 8. Prior to the last imaging session, blood was drawn to assess electrolytes, liver function, and hematology to assess the chronic effects of the high-lipid diet and experimental treatments. All samples were analyzed by Washington University Department of Comparative Medicine.

HISTOLOGY—A separate cohort of atherosclerotic animals (n=7) was utilized for histological determination of $\alpha_v\beta_3$–targeted nanoparticle binding. In one animal, $\alpha_v\beta_3$–targeted rhodamine nanoparticles were injected and allowed to circulate for 3 h. Fifteen minutes prior to sacrifice, fluorescein isothiocyanate (FITC)-labeled lectin was administered intra-arterially. Unbound nanoparticles and lectin were flushed from the vasculature by saline perfusion. The aorta was excised, frozen in OCT medium, sectioned, counterstained with DAPI, and examined with fluorescence microscopy. Adjacent sections were stained with hematoxylin and eosin for light microscopy.

In the remaining animals, MR molecular imaging of angiogenesis was performed with $\alpha_v\beta_3$–targeted paramagnetic nanoparticles, followed by sacrifice and histological measurement of microvessel density. Formalin-fixed samples were paraffin-embedded, sectioned and stained for the expression of $\alpha_v\beta_3$-integrin (LM-609, Chemicon International, Inc.) and PECAM-1 (Chemicon International, Inc.) (18). LM609-positive microvessel density was measured in digitized images from three independent, full transverse sections per animal.

MR molecular imaging of angiogenesis

$\alpha_v\beta_3$–Targeted paramagnetic nanoparticles (1 ml/kg) were injected into the marginal ear vein. Animals were imaged before and three hours after injection with a high-resolution, 2D, T1-weighted, fat suppressed turbo spin echo sequence (250 μm by 250 μm resolution, 4 mm thick slices, TR/TE = 380/11 ms, 90° flip angle, SPIR fat suppression, turbo factor = 4, 6 signal averages, 12.5 minute scan time) using a clinical 1.5 T scanner (Philips Medical Systems, Andover, MA) and a quadrature birdcage coil. Three imaging stacks were acquired covering the descending thoracic aorta (10 slices), the transverse aorta (5 slices) and the ascending

thoracic aorta (5 slices). Saturation bands were positioned superior and inferior to the imaging stacks to suppress signals from in-flowing blood.

MR Image Analysis. MRI signal enhancement from the aortic wall was quantified using a custom, semiautomated segmentation program previously described (17,18). Briefly, the aortic lumen was defined in each 2D image with a seeded region-growing algorithm. The aortic wall was defined by dilation of the luminal mask followed by an automated threshold to obtain a consistent and objective region-of-interest (ROI) encompassing the entire aortic wall (Fig. 1), which was evaluated by visual inspection. Image intensity was normalized across animals and time points to a fiduciary marker (test tube with 25 μmol/L gadolinium diethylene-triamine-pentaacetic acid in saline) placed within the field of view. The percent enhancement in the MR signal was calculated slice-by-slice in the 3-hour post injection images relative to the average preinjection MR signal, providing an unbiased integrated measurement of contrast enhancement in the aortic wall. The aortic contrast data represents the mean enhancement of all properly segmented slices.

Statistical Analysis

All data were analyzed using general linear models (i.e., regression, ANOVA and ANOCOV), and group means for model effects were separated using least-significant differences ($p<0.05$, SAS Inc., Cary, NC) and reported as mean ± standard error of the mean.

RESULTS

Duration of Antiangiogenic Effect After Treatment With $\alpha_v\beta_3$–Integrin Targeted Fumagillin Nanoparticles

At baseline, the average percent signal enhancement from $\alpha_v\beta_3$–targeted paramagnetic nanoparticles did not differ between treatment groups and ranged between 20% and 25% (Fig. 1). Consistent with previous reports, $\alpha_v\beta_3$-targeted paramagnetic contrast was diffusely distributed across and within slices and the enhancement calculated represented the average of all aortic voxels rather than a thresholded subset (17,18). Targeted characterization of $\alpha_v\beta_3$-integrin expression reveals that early MR neovascular signal enhancement did not differ between fat-fed animals switched to standard chow and those continuing on the cholesterol-enriched diet over the four-week study, which reflects the marked serum cholesterol and fatty livers observed in all animals. For clarity of presentation, these treatment groups were pooled (i.e, control).

In the top panel of Figure 2, the overall effects of $\alpha_v\beta_3$–targeted fumagillin nanoparticles on aortic neovascular contrast as a function of post treatment diet are presented. At week one, neovascular contrast among animals receiving $\alpha_v\beta_3$–targeted fumagillin nanoparticles was decreased by approximately 50% to 75% relative to the control animals ($p<0.05$). The decreased neovascular signal persisted through week 2. On week 3, aortic angiogenesis remained less than the control ($p<0.05$) in both dietary groups, but the difference was smaller, indicating that the effect of fumagillin was waning. By week four, there was no difference in the MR neovasculature signal between control and fumagillin treated rabbits regardless of diet. No change ($p>0.05$) in antiangiogenic response profile was found by increasing the fumagillin dose from 30 μg/ml to 90 μg/ml over the four-week period (Fig. 2). Although no difference in antiangiogenic response was appreciated between drug loading levels, the higher dose exhibited a trend toward longer effectiveness when compared to its own signal enhancement at baseline.

Antiangiogenic Synergism of $\alpha_v\beta_3$–Targeted Fumagillin Nanoparticles and Atorvastatin

Consistent with the earlier four-week experiment, the MR signal enhancement from $\alpha_v\beta_3$–targeted paramagnetic nanoparticles averaged between 20% and 25% at baseline (Fig. 3). The neovascular contrast enhancement among hyperlipidemic control rabbits was constant over the eight-week study. Therapy with atorvastatin did not impact the MR angiogenic signal at these time points. The top panel of Figure 3 shows that $\alpha_v\beta_3$–targeted fumagillin nanoparticles elicited the same acute, antiangiogenic response as observed previously in this and in our previous report (18). The first dosage of $\alpha_v\beta_3$–targeted fumagillin nanoparticles decreased the angiogenic signal for two weeks followed by a return to the baseline level after four weeks. The second administration of $\alpha_v\beta_3$–targeted fumagillin nanoparticles mirrored the antiangiogenic effects observed after the first dosage, suggesting that the antineovascular response was not influenced by the preceding drug treatment.

The antiangiogenic effects of atorvastatin alone and in combination with $\alpha_v\beta_3$–targeted fumagillin nanoparticles given once (baseline) or twice (baseline and week 4) are presented in the lower panel of Figure 3. Atorvastatin alone did not effect the MR signal enhancement from the aortic neovasculature over the eight-week study. Administration of dietary atorvastatin and a single dose of $\alpha_v\beta_3$–targeted fumagillin nanoparticles at baseline produced no change in the antiangiogenic response pattern. In addition, continued dietary atorvastatin following fumagillin treatment during the first four-week period did not elicit an antiangiogenic effect during weeks 4 to 8.

Serial treatment with $\alpha_v\beta_3$–targeted fumagillin nanoparticles at baseline and week 4 in conjunction with dietary atorvastatin resulted in the expected pharmacodynamic four-week cyclic pattern observed previously (see Fig. 2). However, the antiangiogenic response to the second dosage of $\alpha_v\beta_3$–targeted fumagillin nanoparticles was sustained by atorvastatin rather than returning to baseline levels. MR neovascular signals on weeks six and eight after the second fumagillin treatment remained at less than half of the baseline contrast levels. While atorvastatin alone exerted no significant effect on plaque angiogenesis in this short study, it is clear that dietary statin therapy can sustain the acute antineovascular benefits of $\alpha_v\beta_3$–targeted fumagillin. The additive effects of fumagillin or statin alone are far less than the synergistic effect of both together. In the ANOVA, this is reflected by the interaction term (statin*fumagillin) $p<0.0001$, signifying a nonparallel response.

Clinical Pathology

Blood samples drawn at the end of the 8-week study were assessed for hematology, electrolyte and liver function (Fig. 4) and compared to laboratory reference ranges published by the University of Minnesota Research Animal Resources program. Leukocyte, hemoglobin, hematocrit and electrolyte (sodium, potassium, and chloride) values were within the normal range for rabbits and did not differ among treatment groups ($p>0.05$). Platelet count averages were similar ($p>0.05$) across treatments (~ 370,000) and elevated somewhat versus the reported normal upper limit for rabbits (270,000), which is considerably lower than the normal limit for other mammalian species.

Alkaline phosphatase (AlkP) was two to three-fold higher than the normal upper limit for all treatment groups, which was numerically highest in the control animals but not statistically different ($p>0.05$). Gamma glutamyltransferase (GGT) was similar among treatment groups ($p>0.05$), but like AlkP, it was numerically highest in the control rabbits. Since a published normal range for GGT in rabbits was unavailable, the normal range for other nonhuman mammals was used. Aspartate aminotransferase (AST) was well within the normal limits and did not differ among treatment groups ($p>0.05$). Alanine aminotransferase (ALT) was increased ($p<0.05$) in rabbits receiving two doses of fumagillin and dietary statin compared to

the normal range and the other treatment groups. Interestingly, the statin only group also showed slightly elevated ALT relative to the control and fumagillin alone groups. While dietary statin combined with a single dose of $\alpha_v\beta_3$–targeted fumagillin nanoparticles elevated ALT higher than either drug alone, the level was not beyond the normal range. Clinical pathology responses were uncorrelated with serum cholesterol level.

The increased AlkP and GGT values and the frank yellow discoloration of rabbit livers noted on necropsy suggested a marked fatty liver pathology without concomitant hepatobiliary disease. The increase in ALT in relation to AST also points to mild, subclinical hepatic insult by statins alone, which are known to induce liver enzyme release, and in combination with the perfluorocarbon nanoparticles, which are predominantly cleared by the liver reticular endothelial cells (21).

Histology

Fluorescence microscopy confirmed that $\alpha_v\beta_3$–targeted rhodamine nanoparticles were distributed in the aortic adventia and were colocalized with FITC-lectin bound to vascular endothelium (Fig. 5). $\alpha_v\beta_3$–targeted rhodamine nanoparticles were not observed in the extravascular regions of the adventia nor within plaque.

The microvascular density followed a logarithmic relationship (R^2=0.84) with the MRI signal enhancement of $\alpha_v\beta_3$-targeted paramagnetic nanoparticles (Fig. 6). Neovascular signal enhancement increased monotonically at higher advential microvessel counts and declined rapidly as neovessel counts decreased.

DISCUSSION

In the present study, we have demonstrated the concept of a prolonged antiangiogenic regimen with potential for clinical translation using a nanomedicine-based strategy, which offers MR molecular imaging for patient stratification and monitoring and targeted drug delivery. Using MR molecular imaging with $\alpha_v\beta_3$–targeted paramagnetic nanoparticles, the pharmacodynamic antiangiogenic effectiveness of single low dose of $\alpha_v\beta_3$–targeted fumagillin nanoparticles was found to persist for three weeks regardless of drug loading after which continued inflammation led to a recrudescence of the neovasculature to baseline levels. Atorvastatin alone did not induce neovascular changes detectable by MR molecular imaging with $\alpha_v\beta_3$–targeted paramagnetic nanoparticles over 8 weeks of study; however, the combination of targeted fumagillin nanoparticles and atorvastatin synergistically sustained the antiangiogenic effect. Microscopic studies corroborated the high correlation between MR signal and neovessel counts and reconfirmed that the $\alpha_v\beta_3$-targeted nanoparticles were constrained to the vasculature of the aortic adventia.

The integrin-targeted nanoparticles incorporated very low dosages of fumagillin, a mycotoxin produced by Aspergillus fumigatus that suppresses angiogenesis by inhibition of methionine aminopeptidase 2 (MetAP2) (22). MetAP2 is responsible for cleavage of the NH_2-terminal methionine residue from nascent proteins (23) and is up-regulated during cellular proliferation (24). TNP-470 is a water-soluble form of fumagillin, which shares the active ovalicin core and analogously inhibits proliferating endothelial cells (i.e., angiogenesis) with little effect on non-endothelial cell types (25). TNP-470 has been studied in human clinical cancer trials and anecdotal cases of disease remission, regression or stabilization have been reported (26,27). Unfortunately, TNP-470 exhibited significant side effects at dosages required for therapeutic effects (60 to 100 mg/kg, serially), including sudden, moderately severe symptoms of neurotoxicity. In the current nanoparticle application, the equivalent dosage of fumagillin (the parent compound) was 10,000-fold less than the total drug dose used in a prior murine ApoE $^{-/-}$ atherosclerotic model (28), yet still achieved remarkable endpoint efficacy. Similarly,

the total gadolinium dose used in these experiments is about 100 times lower than that approved for clinical contrast imaging, which should diminish the potential for nephrogenic systemic fibrosis as reported in patients with advanced renal disease or liver transplantation (29).

Ligand-directed perfluorocarbon nanoparticles are a theranostic (i.e., therapeutic and diagnostic) platform technology targeted in this case to proliferating endothelial cells. The targeted $\alpha_v\beta_3$–integrin is a heterodimeric transmembrane glycoprotein that is differentially up-regulated in proliferating versus quiescent endothelial cells but also expressed by numerous cell types prominently represented in atherosclerotic plaques, including endothelial cells (30, 31), macrophages (32), platelets (33), lymphocytes (33) and smooth muscle cells (34). In this study, fluorescence microscopy demonstrated that perfluorocarbon nanoparticles (250 nm) were confined to endothelial targets within the advential microvasculature at the time of imaging.

The potential role of antiangiogenic therapy in the treatment of atherosclerosis has garnered increasing scientific discussion both pro (15,35) and con (2,36). While there is general agreement that angiogenesis is a prominent feature of vulnerable and ruptured plaques versus more stable fibrocalcific lesions, questions regarding the causative relationship and clinical relevance of antiangiogenic therapeutic strategies in cardiovascular disease have been raised. In this work, we have shown how a theranostic nanomedicine approach can be interwoven with standard clinical practice to provide a sustained antiangiogenic regimen. Moreover, noninvasive MR longitudinal monitoring of atherosclerotic disease with $\alpha_v\beta_3$–targeted paramagnetic particles alone or enhanced with MR intraplaque hemorrhage assessment (37) offers an attractive, quantitative approach to continued medical management, particularly in asymptomatic patients.

Limitations of Study

The utility of the New Zealand White atherosclerotic rabbit model derives from the development of an early-expanded vasa vasorum and neovasculature in response to the lipid infiltrated aortic wall. Unfortunately, many features of human vulnerable plaque are lacking including intraplaque hemorrhage, fibrous cap thinning and plaque rupture. Therefore, important questions surrounding the hypothesis that antiangiogenic treatment will prevent or reduce the incidence of intraplaque hemorrhage as a result of neovessel pruning is poorly addressed in this animal model. Moreover, this model does not develop MRI visible lesions, which precludes the use of MRI with endogenous contrast (37,38) for monitoring plaque size and/or composition, while other animal models involving balloon injury, de-endothelialation and genetic modifications more closely mimic certain pathology features of vulnerable plaques, such as large lipid cores. None of the models compatible with nanoparticle research fully embrace the morphologic complexity and biochemical interplay of the human atherosclerotic plaque.

Additionally, hyperlipidemic rabbits suffer increased morbidity beyond 150 days on chronic cholesterol diet, which precluded determining the long-term duration of reduced angiogenesis achieved in the group receiving fumagillin (2x) and statin. Finally, one might reasonably speculate that a single dose of fumagillin following a month of statin treatment could yield a similar sustained reduction of atherosclerotic angiogenesis, which would be more desirable from a patient safety, compliance, and healthcare cost perspectives.

Although we did not repeat competitive binding studies in these experiments due to logistic constraints, we have demonstrated previously that these $\alpha_v\beta_3$–targeted nanoparticle bind specifically to the neovascular endothelium with high affinity and avidity (17). The reproducibility of the present and previous MR imaging results and the targeted antiangiogenic effects over multiple cohorts of rabbits, together with the “washout” studies showing

recrudescence without continued therapy followed by efficacy upon retreatment corroborate the robustness of this agent for diagnostic imaging and targeted drug delivery *in vivo*.

Conclusions

Others have postulated that antiangiogenesis therapy may normalize atherosclerotic plaque vasculature through neovascular pruning, which could diminish intraplaque hemorrhage frequency and promote plaque stabilization. The overarching hypothesis of these studies was to determine whether the acute antiangiogenic effects of $\alpha_v\beta_3$–targeted fumagillin nanoparticles could be incorporated into a clinically translatable regimen for testing the potential benefits of long-term antineovascular therapy. MR molecular imaging with $\alpha_v\beta_3$–targeted paramagnetic nanoparticles was used to noninvasively demonstrate that a single minute dose of $\alpha_v\beta_3$–targeted fumagillin nanoparticles decreased aortic angiogenesis for three weeks and this effect was prolonged with the addition of atorvastatin. This theranostic nanomedicine approach could translate into a clinically relevant strategy to evaluate prolonged antiangiogenic treatment and atherosclerotic plaque stability.

Acknowledgements

We extend sincere appreciation to Grace Hu for analytical support, to Ralph Fuhrhop and Elizabeth Lacy for formulation chemistry, to John Allen and Cordelia Caradine for their assistance with the rabbit model, and to Michael Scott for program management support.

Sources of Funding This work was supported in part by the National Cancer Institute, National Heart Lung and Blood Institute and the National Institute for Biomedical Imaging and Bioengineering (HL-78631, HL-73646, N01-CO-37007, N01-CO-27031-16, CA-119342 and EB-01704) and Philips Healthcare and Philips Research.

References

1. Moreno PR, Purushothaman KR, Fuster V, et al. Plaque neovascularization is increased in ruptured atherosclerotic lesions of human aorta: Implications for plaque vulnerability. Circulation 2004;110:2032–2038. [PubMed: 15451780]
2. Moreno PR, Purushothaman KR, Sirol M, Levy AP, Fuster V. Neovascularization in human atherosclerosis. Circulation 2006;113:2245–2252. [PubMed: 16684874]
3. Virmani R, Kolodgie FD, Burke AP, et al. Atherosclerotic plaque progression and vulnerability to rupture: Angiogenesis as a source of intraplaque hemorrhage. Arterioscler Thromb Vasc Biol 2005;25:2054–2061. [PubMed: 16037567]
4. Bjornheden T, Levin M, Evaldsson M, Wiklund O. Evidence of hypoxic areas within the arterial wall in vivo. Arterioscler Thromb Vasc Biol 1999;19:870–876. [PubMed: 10195911]
5. Boyle JJ, Wilson B, Bicknell R, Harrower S, Weissberg PL, Fan TP. Expression of angiogenic factor thymidine phosphorylase and angiogenesis in human atherosclerosis. J Pathol 2000;192:234–42. [PubMed: 11004701]
6. Khatri J, Johnson C, Magid R, et al. Vascular oxidant stress enhances progression and angiogenesis of experimental atheroma. Circulation 2004;109:520–525. [PubMed: 14744973]
7. de Boer OJ, van der Wal AC, Teeling P, Becker AE. Leucocyte recruitment in rupture prone regions of liid-rich plaques: a prominent role for neovascularization? Cardiovasc Res 1999;41:443–449. [PubMed: 10341843]
8. Pasternak RC, Smith SC Jr, Bairey-Merz CN, Grundy SM, Cleeman JI, Lenfant C. ACC/AHA/NHLBI clinical advisory on the use and safety of statins. Circulation 2002;106:1024–8. [PubMed: 12186811]
9. Girona J, La Ville AE, Sola R, Plana N, Masana L. Simvastatin decreases aldehyde production derived from lipoprotein oxidation. Am J Cardiol 1999;83:846–51. [PubMed: 10190397]
10. Kimura M, Kurose I, Russell J, Granger DN. Effects of fluvastatin on leukocyte-endothelial cell adhesion in hypercholesterolemic rats. Arterioscler Thromb Vasc Biol 1997;17:1521–6. [PubMed: 9301630]

11. Verhoeven BA, Moll FL, Koekkoek JA, et al. Statin treatment is not associated with consistent alterations in inflammatory status of carotid atherosclerotic plaques: a retrospective study in 378 patients undergoing carotid endarterectomy. Stroke 2006;37:2054–60. [PubMed: 16809559]
12. Laufs U, La Fata V, Plutzky J, Liao JK. Upregulation of endothelial nitric oxide synthase by HMG CoA reductase inhibitors. Circulation 1998;97:1129–1135. [PubMed: 9537338]
13. Sukhova GK, Williams JK, Libby P. Statins reduce inflammation in atheroma of nonhuman primates independent of effects on serum cholesterol. Arterioscler Thromb Vasc Biol 2002;22:1452–1458. [PubMed: 12231565]
14. Koutouzis M, Nomikos A, Nikolidakis S, et al. Statin treated patients have reduced intraplaque angiogenesis in carotid endarterectomy specimens. Atherosclerosis 2007;192:457–63. [PubMed: 17335827]
15. Kolodgie FD, Narula J, Yuan C, Burke AP, Finn AV, Virmani R. Elimination of neoangiogenesis for plaque stabilization: is there a role for local drug therapy? J Am Coll Cardiol 2007;49:2093–101. [PubMed: 17531658]
16. Kamba T, McDonald DM. Mechanisms of adverse effects of anti-VEGF therapy for cancer. Br J Cancer 2007;96:1788–95. [PubMed: 17519900]
17. Winter PM, Morawski AM, Caruthers SD, et al. Molecular imaging of angiogenesis in early-stage atherosclerosis with alpha(v)beta3-integrin-targeted nanoparticles. Circulation 2003;108:2270–4. [PubMed: 14557370]
18. Winter P, Neubauer A, Caruthers S, et al. Endothelial alpha(nu)beta(3)-Integrin targeted fumagillin nanoparticles inhibit angiogenesis in atherosclerosis. Arterioscler Thromb Vasc Biol 2006;26:2103–2109. [PubMed: 16825592]
19. Winter PM, Schmieder AH, Caruthers SD, et al. Minute dosages of alpha(nu)beta(3)-targeted fumagillin nanoparticles impair Vx-2 tumor angiogenesis and development in rabbits. FASEB J. 2008In Press
20. Sadeghi MM, Krassilnikova S, Zhang J, et al. Detection of injury-induced vascular remodeling by targeting activated alphavbeta3 integrin in vivo. Circulation 2004;110:84–90. [PubMed: 15210600]
21. Hu G, Lijowski M, Zhang H, et al. Imaging of Vx-2 rabbit tumors with alpha(nu)beta3-integrin-targeted 111In nanoparticles. Int J Cancer 2007;120:1951–7. [PubMed: 17278104]
22. Liu S, Widom J, Kemp CW, Crews CM, Clardy J. Structure of human methionine aminopeptidase-2 complexed with fumagillin. Science 1998;282:1324–7. [PubMed: 9812898]
23. Arfin SM, Kendall RL, Hall L, et al. Eukaryotic methionyl aminopeptidases: two classes of cobalt-dependent enzymes. Proc Natl Acad Sci U S A 1995;92:7714–8. [PubMed: 7644482]
24. Wang J, Lou P, Henkin J. Selective inhibition of endothelial cell proliferation by fumagillin is not due to differential expression of methionine aminopeptidases. J Cell Biochem 2000;77:465–73. [PubMed: 10760954]
25. Griffith EC, Su Z, Niwayama S, Ramsay CA, Chang YH, Liu JO. Molecular recognition of angiogenesis inhibitors fumagillin and ovalicin by methionine aminopeptidase 2. Proc Natl Acad Sci U S A 1998;95:15183–8. [PubMed: 9860943]
26. Bhargava P, Marshall JL, Rizvi N, et al. A Phase I and pharmacokinetic study of TNP-470 administered weekly to patients with advanced cancer. Clin Cancer Res 1999;5:1989–95. [PubMed: 10473076]
27. Kudelka AP, Verschraegen CF, Loyer E. Complete remission of metastatic cervical cancer with the angiogenesis inhibitor TNP-470. N Engl J Med 1998;338:991–2. [PubMed: 9527612]
28. Moulton KS, Heller E, Konerding MA, Flynn E, Palinski W, Folkman J. Angiogenesis inhibitors endostatin or TNP-470 reduce intimal neovascularization and plaque growth in apolipoprotein E-deficient mice. Circulation 1999;99:1653–5. [PubMed: 10190871]
29. Broome DR. Nephrogenic systemic fibrosis associated with gadolinium based contrast agents: A summary of the medical literature reporting. Eur J Radiol. 2008
30. Cheresh DA. Integrins in thrombosis, wound healing and cancer. Biochem Soc Trans 1991;19:835–8. [PubMed: 1794568]
31. Friedlander M, Theesfeld CL, Sugita M, et al. Involvement of integrins alpha v beta 3 and alpha v beta 5 in ocular neovascular diseases. Proc Natl Acad Sci U S A 1996;93:9764–9. [PubMed: 8790405]

32. De Nichilo M, Burns G. Granulocyte-macrophage and macrophage colony-stimulating factors differentially regulate alpha v integrin expression on cultured human macrophages. Proc Natl Acad Sci U S A 1993;90:2517–2521. [PubMed: 7681600]

33. Helluin O, Chan C, Vilaire G, Mousa S, DeGrado WF, Bennett JS. The activation state of alphavbeta 3 regulates platelet and lymphocyte adhesion to intact and thrombin-cleaved osteopontin. J Biol Chem 2000;275:18337–43. [PubMed: 10751402]

34. Itoh H, Nelson P, Mureebe L, Horowitz A, Kent K. The role of integrins in saphenous vein vascular smooth muscle cell migration. J Vasc Surg 1997;25:1061–9. [PubMed: 9201167]

35. Doyle B, Caplice N. Plaque Neovascularization and Antiangiogenic Therapy for Atherosclerosis. J Am Coll Cardiol 2007;49:2073–2080. [PubMed: 17531655]

36. Khurana R, Simons M, Martin JF, Zachary IC. Role of angiogenesis in cardiovascular disease: A critical appraisal. Circulation 2005;112:1813–1824. [PubMed: 16172288]

37. Takaya N, Yuan C, Chu B, et al. Presence of intraplaque hemorrhage stimulates progression of carotid atherosclerotic plaques: a high-resolution magnetic resonance imaging study. Circulation 2005;111:2768–75. [PubMed: 15911695]

38. Raman SV, Winner MW, Tran T, et al. In vivo atherosclerotic plaque characterization using magnetic susceptibility distinguishes symptom-producing plaques. J Am Coll Cardiol Img 2008;1:49–57.

Selected Abbreviations

AlkP
: Alkaline phosphatase

ALT
: Alanine aminotransferase

AST
: Aspartate aminotransferase

GGT
: Gamma glutamyltransferase

IC_{50}
: half maximal inhibitory concentration

MetAP2
: methionine aminopeptidase 2

MR
: magnetic resonance

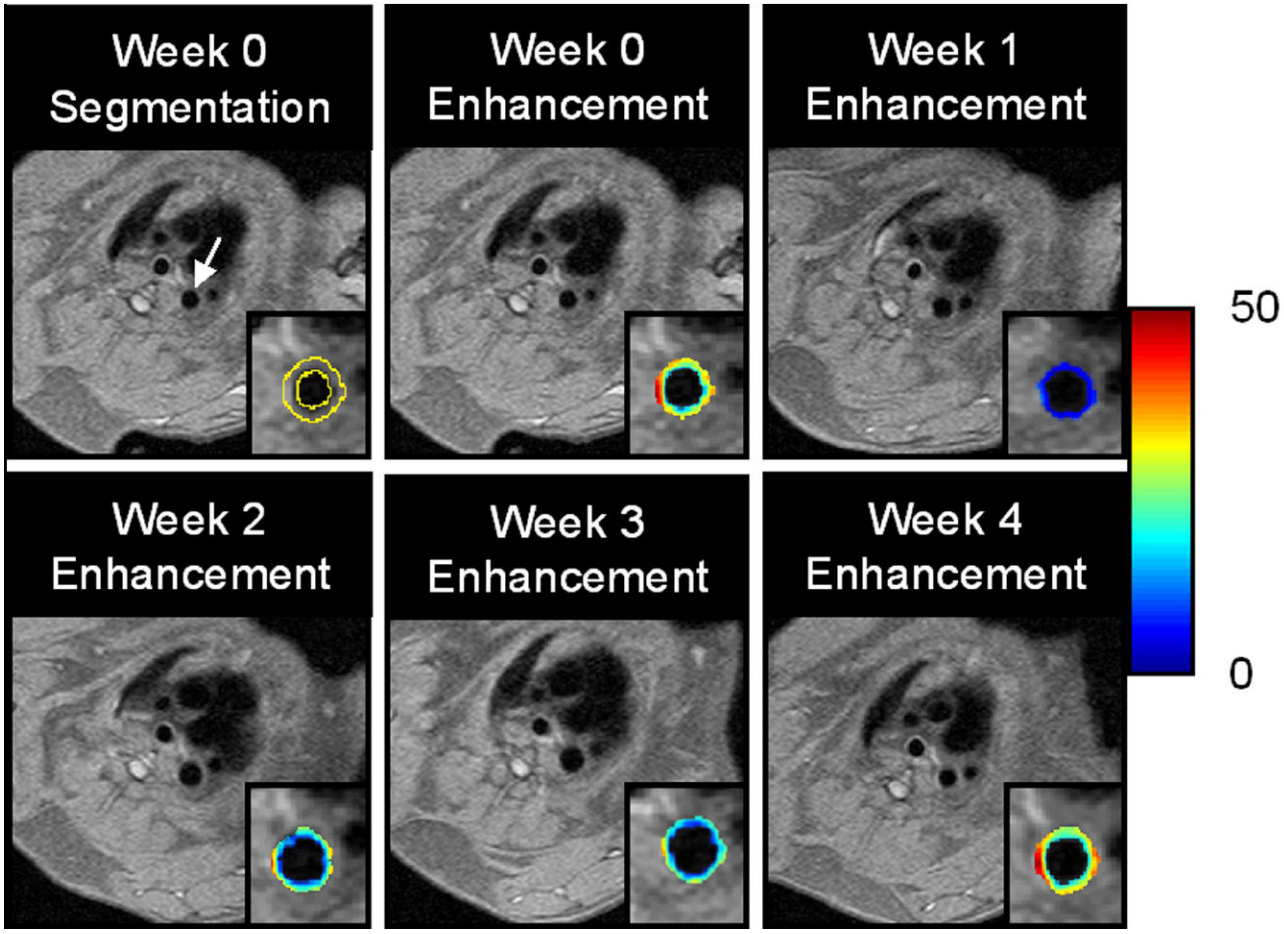

Figure 1. Segmentation of the Aortic Wall and Color-Coded Signal Enhancement Before and After Targeted Fumagillin Treatment

TOP: Black blood image of the thoracic aorta (arrow) and segmentation of the vessel wall (outlined in yellow) is shown for the week 0 image. The color-coded overlay of signal enhancement (in percent) shows patchy areas of high angiogenesis. On the week 1 image, the signal enhancement has clearly decreased due to the antiangiogenic effect of targeted fumagillin treatment. BOTTOM: The level of signal enhancement gradually increases at weeks 2 and 3 after fumagillin treatment, until week 4 where the level of enhancement is practically identical to the week 0 image.

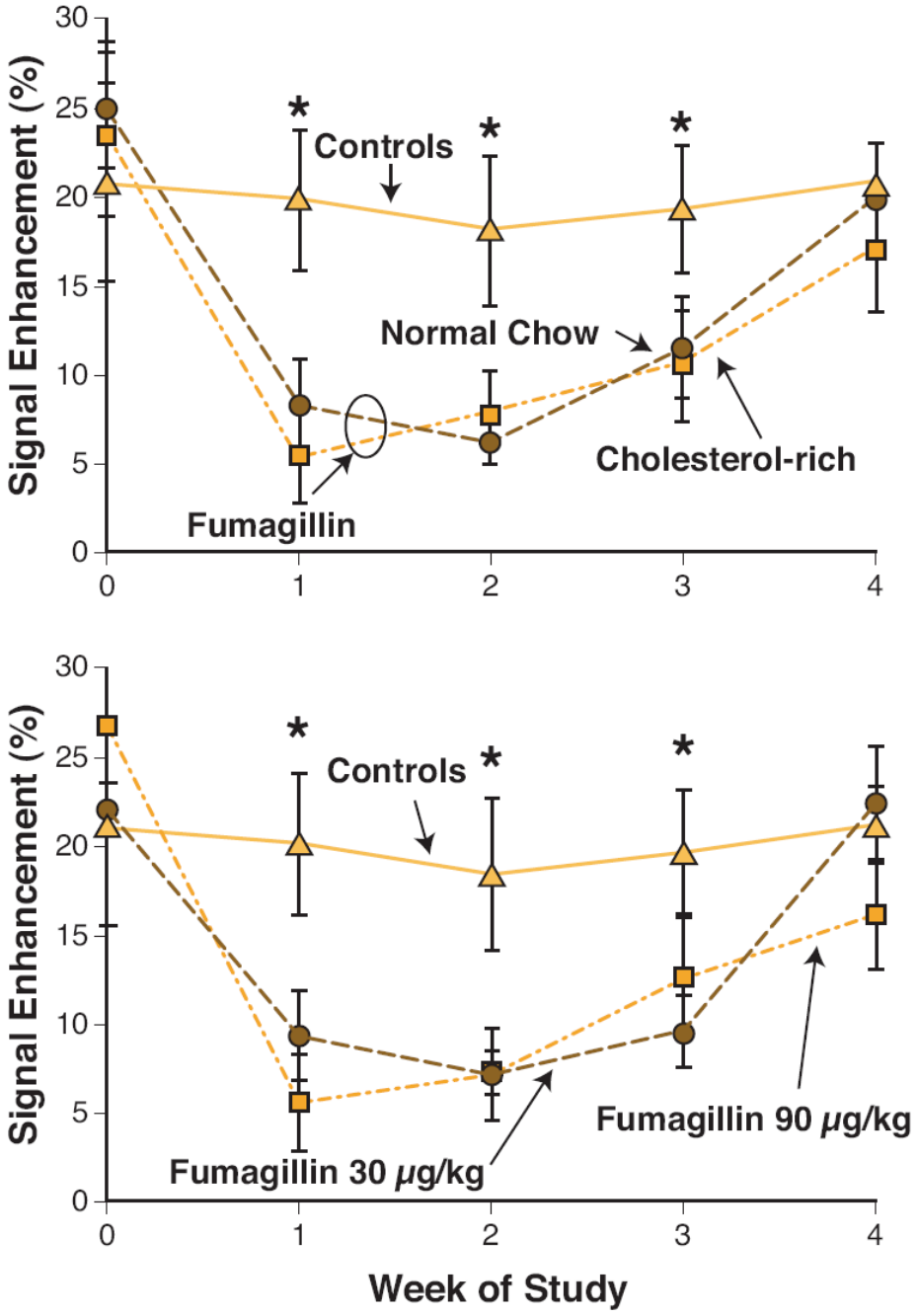

Figure 2. Aortic Signal Enhancement up to Four Weeks Post Treatment with Targeted Fumagillin Nanoparticles

TOP: Serial imaging of angiogenesis in untreated (▲) and fumagillin treated animals remaining on high cholesterol diet (■) or switched to normal chow (●). Image enhancement in the fumagillin treatment at week 0 reduced angiogenesis compared to untreated controls (*$p<0.05$), but withdrawing the high-cholesterol feed had no effect. BOTTOM: Aortic angiogenesis in rabbits without treatment (▲), 30 μg/kg fumagillin (●) or 90 μg/kg fumagillin (■). Fumagillin treatment at 30 vs. 90 μg/kg produced identical responses. (*$p<0.05$)

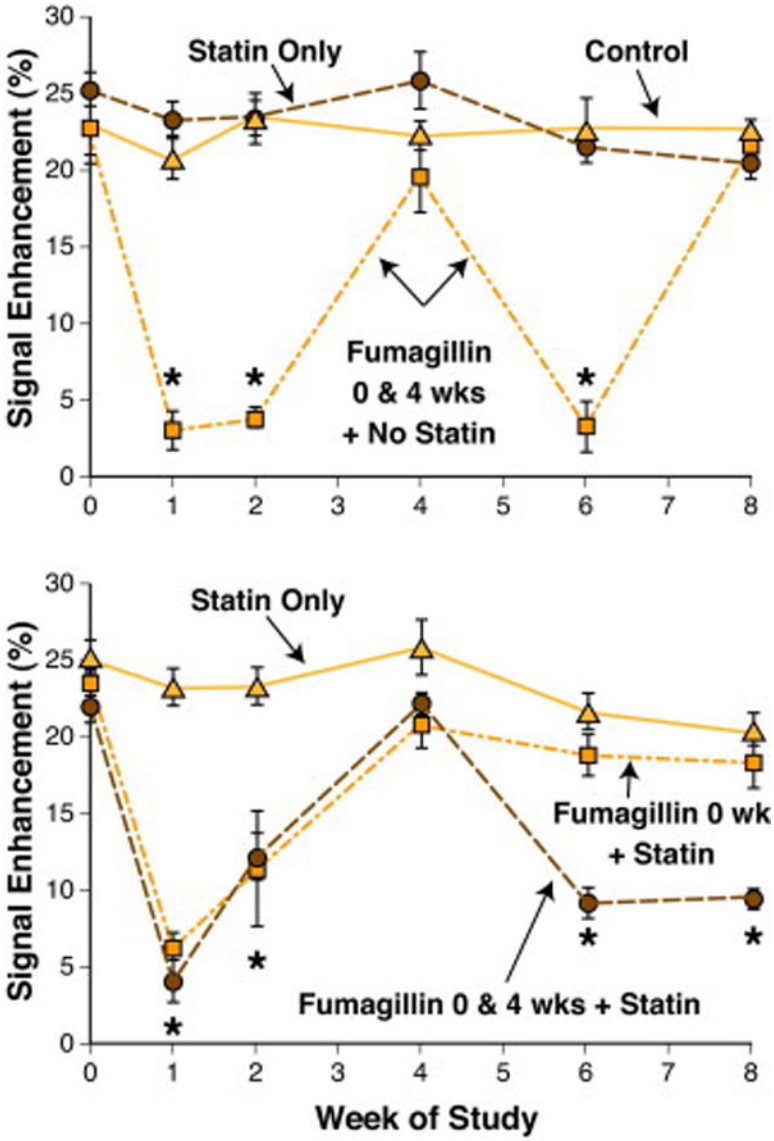

Figure 3. MR Signal Enhancement up to Eight Weeks Post Treatment with Targeted Fumagillin Nanoparticles With and Without Oral Atorvastatin

TOP: MRI enhancement in untreated (▲), atorvastatin treated (●) and fumagillin treated animals (■) during 8 weeks of follow-up imaging. Untreated and statin treated animals showed a constant level of angiogenesis in the aortic wall. Animals treated with targeted fumagillin nanoparticles at weeks 0 and 4 (0 & 4 wks) showed decreased angiogenesis (*$p<0.05$) following each dose, which returned to baseline levels within 4 weeks. BOTTOM: Enhancement in rabbits receiving atorvastatin alone (▲) or in conjunction with one (■) or two (●) doses of targeted fumagillin nanoparticles. The combination of two fumagillin doses and statin produced a sustained decrease in angiogenesis (*$p<0.05$).

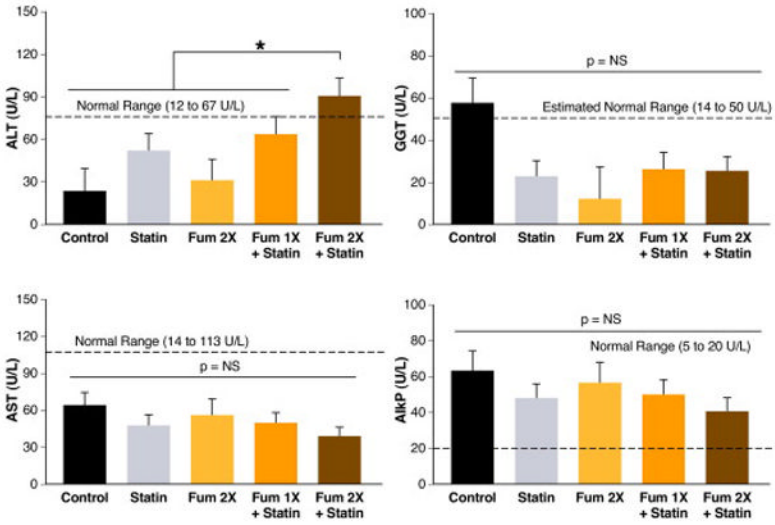

Figure 4. Liver Function Enzymes After Eight Weeks of Atorvastatin Treatment With or Without Targeted Fumagillin Nanoparticles

Blood samples drawn at the end of the 8-week study were assessed for liver function enzymes to assess the chronic effects of the high-lipid diet and experimental treatments. All values tended to be within normal ranges and identical for all treatment groups. Alkaline phosphate (AlkP), however, was elevated in all groups and alanine aminotransferase (ALT) was increased in animals receiving two doses of targeted fumagillin nanoparticles and oral statin (Fum 1x + Statin) (*$p<0.05$). AST = aspartate aminotransferase; GGT = gamma glutamyltransferase; NS = not significant.

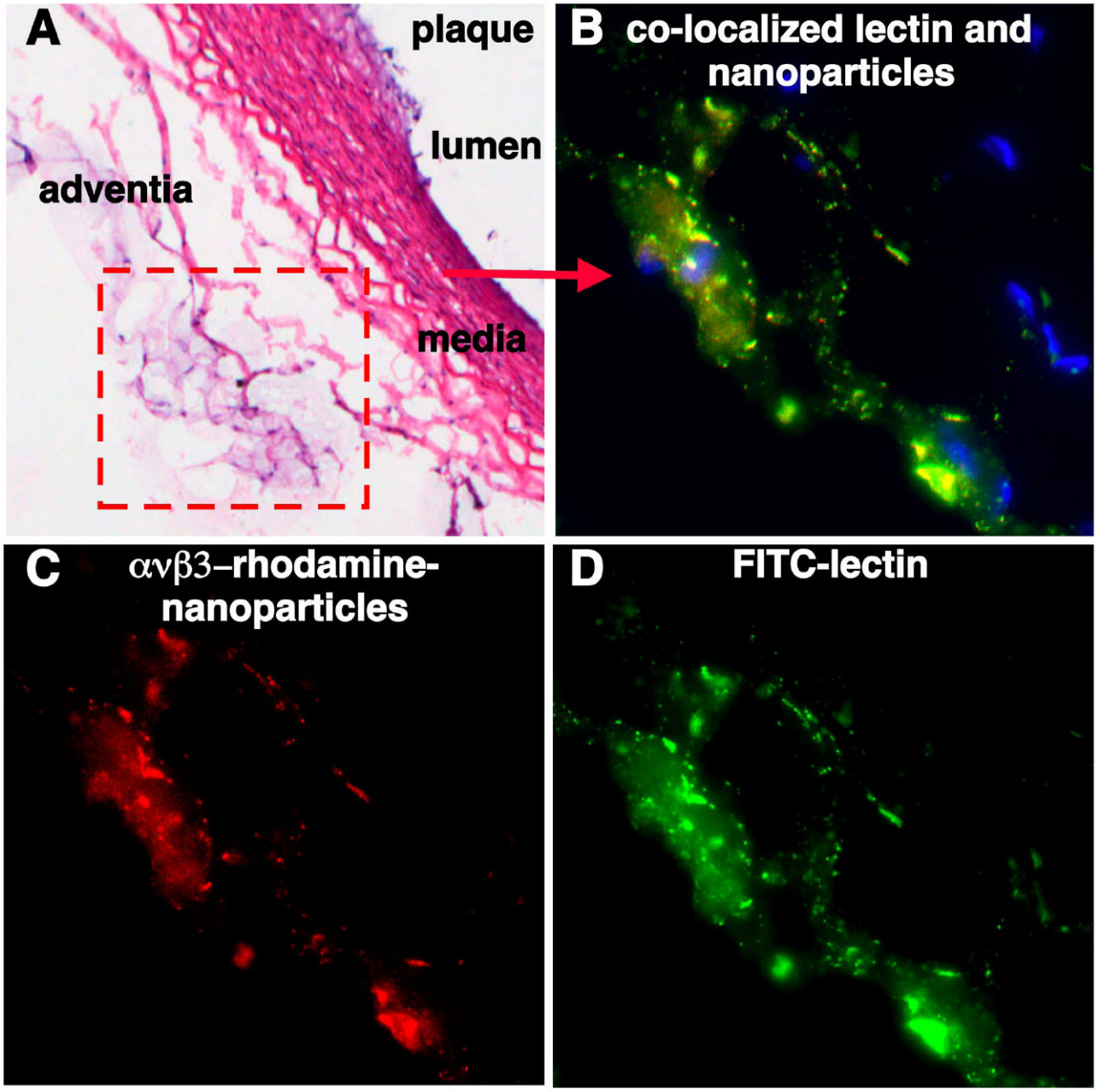

Figure 5. $\alpha_v\beta_3$–Targeted Nanoparticles Bind to the Advential Vasculature

Routine light microscopy and fluorescence microscopy of $\alpha_v\beta_3$–targeted rhodamine nanoparticles and fluorescein isothiocyanate (FITC) labeled lectin, a vascular endothelial marker, enables localization of nanoparticle binding with respect to normal and pathological vascular structures. (A) Hematoxylin and eosin (H&E) staining of aorta shows small plaque, media and adventia (10x). (B) High power fluorescent image demonstrates co-localization of rhodamine labeled $\alpha_v\beta_3$-targeted nanoparticles (shown in C, 60x) with FITC labeled lectin (shown in D, 60x), indicating that the nanoparticles are vascularly constrained to the neovessels of the adventitia. No rhodamine labeled $\alpha_v\beta_3$-targeted nanoparticles were appreciated in the lumen plaque (not shown).

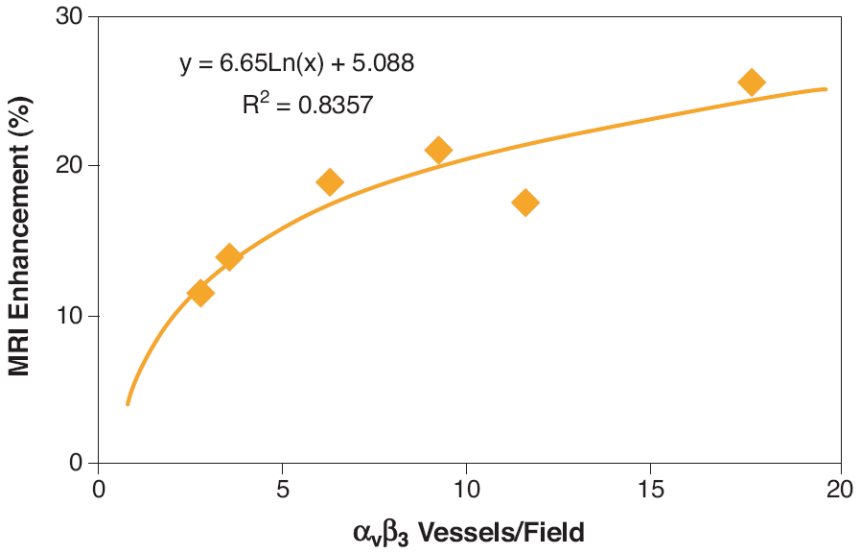

Figure 6. MRI Enhancement with $\alpha_v\beta_3$-Targeted Nanoparticles Correlates to the Density of Angiogenic Microvessels

MR molecular imaging of angiogenesis with $\alpha_v\beta_3$-targeted paramagnetic nanoparticles and histological measurement of microvessel density was performed on a separate cohort of atherosclerotic rabbits. Aortic sections were stained for $\alpha_v\beta_3$-integrin (LM-609) and PECAM (Platelet Endothelial Cell Adhesion Molecule), a general vascular marker. The number of microvessels expressing both $\alpha_v\beta_3$-integrin and PECAM were counted in three independent, full transverse sections per animal. The number of angiogenic microvessels per high powered field was correlated in a logarithmic fashion ($R^2 = 0.84$) to the MRI signal enhancement observed after injection of $\alpha_v\beta_3$-targeted particles.